Available online at www.sciencedirect.com
ScienceDirect
Neurocomputing 71 (2007) 3–12
NEUROCOMPUTING
www.elsevier.com/locate/neucom

A subthreshold CMOS circuit for a piecewise linear neuromorphic oscillator with current-mode low-pass filters

Kazuki Nakada[a,*], Tetsuya Asai[b], Tetsuya Hirose[b], Hatsuo Hayashi[a], Yoshihito Amemiya[b]

[a]Graduate School of Life Science and Systems Engineering, Kyushu Institute of Technology, Kitakyushu, Fukuoka 808-0196, Japan
[b]Graduate School of Information Science and Technology, Hokkaido University, Sapporo, Hokkaido 060-0814, Japan

Received 12 May 2006; received in revised form 25 November 2006; accepted 29 November 2006
Available online 20 July 2007

Abstract

We propose an analog current-mode subthreshold CMOS circuit implementing a piecewise linear neuromorphic oscillator. Our circuit was derived from a piecewise linear oscillator model proposed by Matsuoka, well known as a building block for constructing a robot locomotion controller. We modified Matsuoka's oscillator to be suitable for analog current-mode integrated circuit implementation, and designed and fabricated it as an analog current-mode circuit. Through circuit simulations and experimental results on a fabricated chip, we demonstrate that our neuromorphic oscillator generates a stable oscillation, and the amplitude and frequency of the oscillation can be controlled by tuning bias currents over a wide range. Further, we propose a compensation for device mismatch in the neuromorphic oscillator through feedback from a coupled physical system.

Keywords: Analog subthreshold CMOS circuit; Current-mode implementation; Neuromorphic oscillator; Locomotion control; Feedback loop

1. Introduction

Fundamental rhythmic movements for locomotor behavior of animals, such as walking, running, flying, and swimming, are generated by part of the central nervous system called the central pattern generator (CPG) [8]. Induced by inputs from a higher level, a CPG generates rhythmic neural activity activating muscles in the absence of any sensory inputs, resulting in locomotor behavior of animals. While not necessary for generating rhythmic activity, sensory inputs regulate such rhythmic activity over a wide range. As a result, locomotor behavior of animals can be adapted to unpredictable environments [12].

From a point of view of nonlinear dynamics, it is explained that rhythmic movements during locomotion emerge as a stable limit cycle from mutual entrainment between the neural system that includes the CPG and the physical system that interacts with a varying environment through sensory feedback [31]. Such entrainment, termed *global entrainment*, induces high adaptation to unpredictable environments [31].

For utilizing *global entrainment* to control locomotor behavior of robots, many researchers have dedicated efforts to designing locomotion controllers based on CPG (e.g., [3,11,13,14,16,20,24,25,30,31,33]). Taga et al. have used a CPG model constructed from the neural oscillator model proposed by Matsuoka [17] in simulating for biped locomotion [31]. Kimura et al. have used a CPG model for quadruped robot locomotion on rough terrain [13]. Williamson has applied a CPG model for controlling rhythmic arm movements of a humanoid robot [33].

Such CPG models consist of coupled nonlinear oscillators, each of which generates rhythmic activity for actuating each joint of the limbs. Functions of a CPG model depend on both dynamical properties of a nonlinear oscillator as a component and its coupling topology. Collins et al. [7] and Golubitsky [9] have shown common properties of CPG models consisting of different types of nonlinear oscillators, e.g., symmetry-breaking bifurcation [9], that only depends on their coupling topology. However, recent

*Corresponding author. Tel.: +81 90 8898 4080.
E-mail addresses: nakada@brain.kyutech.ac.jp (K. Nakada), asai@sapiens-ei.eng.hokudai.ac.jp (T. Asai), hirose@sapiens-ei.eng.hokudai.ac.jp (T. Hirose), hayashi@brain.kyutech.ac.jp (H. Hayashi), amemiya@sapiens-ei.eng.hokudai.ac.jp (Y. Amemiya).

0925-2312/$ - see front matter © 2007 Elsevier B.V. All rights reserved.
doi:10.1016/j.neucom.2006.11.026

findings suggest that nonlinear phenomena, such as flexible phase-locking [25] and phase resetting [24], play key roles in utilizing sensory feedback effectively for high adaptation during locomotion. These phenomena depend on intrinsic properties of nonlinear oscillators underlying a CPG model.

In neuromorphic engineering, many CPG models have been implemented into silicon chips [2,5,15,22,23,26–29,32]. As a building block for a CPG chip, using a neuromorphic oscillator to control the amplitude and frequency of the oscillation over a wide range is desirable because entrainment properties of CPG chips rely on a dynamic range of a neuromorphic oscillator, and such entrainment properties are also significant for utilizing sensor feedback effectively.

The aim of this work is to implement a neuromorphic oscillator with high controllability of the amplitude and frequency of oscillation. We focused on the piecewise linear oscillator model proposed by Matsuoka that provides scalability of the amplitude of oscillation [17] because such scalability has an advantage for reflecting sensory feedback in rhythmic pattern generation [13,30,31]. For using the scalability effectively, we revised the model slightly, and implemented it as an analog subthreshold CMOS circuit using current-mode representation with a wide dynamic range [1]. Through SPICE simulations and experiments on a fabricated chip, we demonstrated that our circuit can generate a stable oscillation of currents, and the amplitude and frequency of the oscillation can be controlled over a wide range by tuning bias currents. Further, we propose a method to compensate device mismatch effects in a neuromorphic oscillator exploiting sensory feedback from a coupled physical system.

The present paper is organized as follows. In Section 2, we introduce a piecewise linear oscillator model suitable for analog current-mode integrated circuit implementation. In Section 3, we describe an analog current-mode circuit for the piecewise linear oscillator model. We demonstrated the performance of our neuromorphic oscillator through circuit simulations and experiments that we describe in Section 4. We also describe a method to compensate device mismatch effects exploiting physical feedback in Section 5. A summary of this paper is presented in Section 6.

2. Piecewise linear oscillator models

Let us here describe two piecewise linear oscillator models based on the concept of the half-center oscillator in the field of neuroscience. One has been frequently used as a component of a CPG-based controller in robotics. Another is a version of the previous model revised to be suitable for analog integrated circuit implementation by using current-mode representation.

2.1. Biological concept of half-center oscillator

We here briefly review the biological concept of the half-center oscillator to account for alternating rhythmic activity in flexor and extensor motoneurons in locomotion of animals [6]. Fig. 1 shows the half-center oscillator model proposed by Brown, which consists of two neurons; a flexor half-center and an extensor half-center, each is connected with reciprocal inhibition. The half-centers alternatively activate flexor and extensor motoneurons in the absence of any pacemaker cells. Each half-center has dynamical properties, such as self-inhibition, fatigue or adaptation. The flexor half-center activates the flexor muscles and suppresses the extensor half-center via synaptic inhibition in the flexion phase; in turn, transition from the flexion phase to extension phase occurs due to the self-inhibition and adaptation. As in the case of the flexion phase, the extensor half-center activates the extensor muscles and suppresses the flexor half-center in the extension phase.

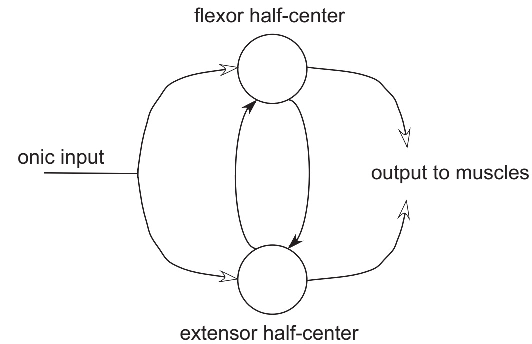

Fig. 1. Conceptual illustration of half-center oscillator.

2.2. Half-center oscillator model with piecewise linearity

Matsuoka proposed a half-center oscillator model consisting of two neurons with piecewise linearity. The dynamics of the half-center oscillator model are described by the following system equations [17]:

$$\tau_u \frac{\mathrm{d}u_i}{\mathrm{d}t} = -u_i + s - \beta v_i - w_{ij} f(u_j), \tag{1}$$

$$\tau_v \frac{\mathrm{d}v_i}{\mathrm{d}t} = -v_i + f(u_i), \tag{2}$$

where u_i represents the inner state of the ith neuron, v_i an adaptation variable of the ith neuron ($i = 1, 2$), s a tonic input, w_{ij} a synaptic strength between the ith and jth neuron, β the adaptation effectiveness, τ_u a time constant of the self-inhibition, and τ_v a time constant of the adaptation effect. The nonlinearity of this model is given in the form of a piecewise linear function

$$f(x) = \max(0, x), \tag{3}$$

where f corresponds to the output of a neuron. Depending on the parameters, this model has a stable limit-cycle oscillation. The stability and dynamical properties of this model are analyzed in detail [4,10,17,18]. The amplitude of the oscillation is proportional to the tonic input s due to the piecewise linearity, in other words, the amplitude of the oscillation is scalable. The frequency and shape of the oscillation can also be controlled by tuning the ratio of time constants. These properties are well suited for controlling rhythmic movements of a robot. In particular, the scalability of the amplitude of the oscillation is appropriate for utilizing sensory feedback [31] that plays critical roles in adapting rhythmic movements to unexpected environments [8]. Focusing on such properties, this model has been fluently used in robotics [13,30,31]. Taga et al. have used it in simulating biped locomotion [31]. Kimura et al. have applied it to control a quadruped walking robot on rough terrain [13]. Williamson has applied it to control robot arm movements [33].

Fig. 2A shows closed (u_1, v_1) phase plane portraits of Matsuoka's model for different tonic inputs, $s = 0.5, 1.5$, and 2.5, where we set the parameters as follows: $\beta = 3.5$, $w_{ij} = 2.5$, and $\tau_u = \tau_v = 2.5$. We confirmed that the amplitude of the oscillations were proportional to the tonic inputs.

2.3. Piecewise linear half-center oscillator model for circuit implementation

We here introduce a piecewise linear half-center oscillator model for analog current-mode circuit implementation. For effectively utilizing the scalability of the amplitude of oscillation of Matsuoka's model, we consider implementing it into a silicon chip by using current-mode representation with a wide dynamic range. However, it should be noted that the state variables of Matsuoka's model, u_i and v_i, can be both positive and negative, as shown in Fig. 2A. For simplicity, such state variables are desirable not to have polarity because to represent a state variable with polarity using uni-directional currents is complex. To avoid complexity in current-mode circuit implementation, we revised Matsuoka's model slightly as follows:

$$\tau_u \frac{du_i}{dt} = -u_i + f(s - \beta v_i - w_{ij} u_j), \tag{4}$$

$$\tau_v \frac{dv_i}{dt} = -v_i + f(u_i), \tag{5}$$

where all variables and parameters are same as in (1)–(2), and the nonlinear function f is the same as the piecewise linear function given by (3). In this model, when u_i becomes very close to 0, the derivative of u_i with regard to t turns to positive. As a result, we can obtain a limit-cycle solution such that all state variables are positive. Fig. 2B shows closed (u_1, v_1) phase plane portraits of the revised model for different tonic inputs, $s = 0.5, 1.5$, and 2.5, where we set the parameters as follows: $\beta = 5$, $w_{ij} = 4$, and $\tau_u = \tau_v = 2.5$. Thus, this model is suitable to be implemented as an analog current-mode circuit that treats uni-directional currents.

3. Circuit implementation

We here propose an analog current-mode integrated circuit for the piecewise linear half-center oscillator model described in the previous section.

Fig. 3 is a block diagram of the half-center oscillator model that consists of four low-pass filters and four piecewise linear functions. The low-pass filters can be implemented with a current-mode low-pass filter operating in log-domain based on the dynamic translinear principle [19,21]. Fig. 4 is a schematic of the current-mode low-pass filter. The circuit dynamics are expressed by the following

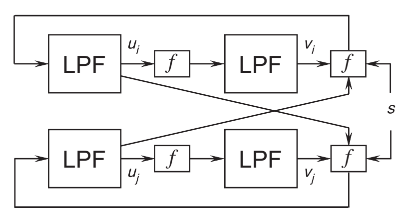

Fig. 3. Block diagram of the revised piecewise linear half-center oscillator model.

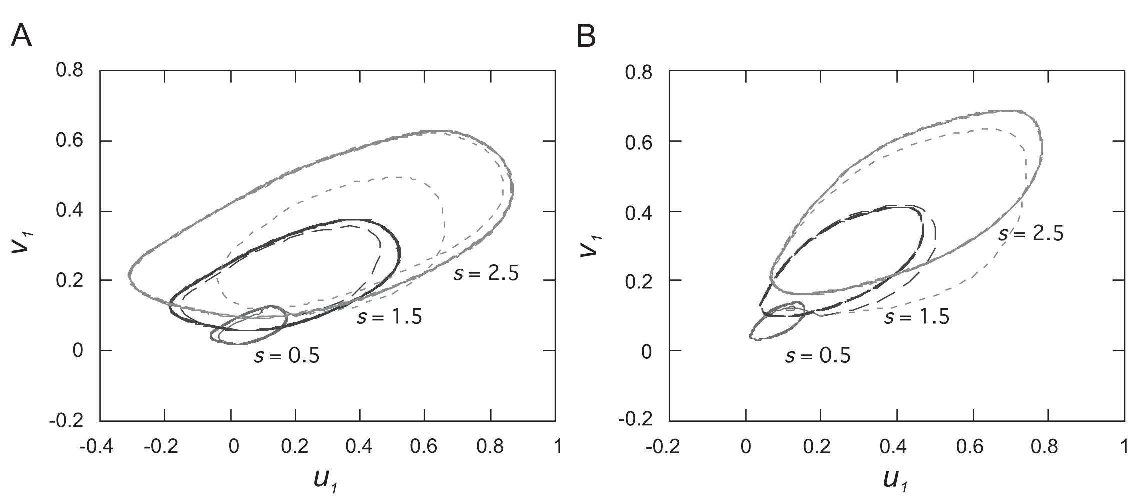

Fig. 2. Phase plane portraits of (A) the half-center oscillator model proposed by Matsuoka and (B) a revised version for analog current-mode circuit implementation.

equation:

$$\tau \frac{\mathrm{d}I_{\mathrm{out}}}{\mathrm{d}t} = -I_{\mathrm{out}} + I_{\mathrm{in}}, \tag{6}$$

where I_{in} represents the input current, I_{out} the output current, and τ the time constant, which is expressed by

$$\tau = \frac{CU_{\mathrm{T}}}{I_\tau}, \tag{7}$$

where C represents the capacitance, U_{T} the thermal voltage, and I_τ the bias current. The low-pass characteristics with respect to the output current I_{out} are derived from the currents relationship as a result of a translinear loop formed by M1–M4 and dynamic translinear circuits including M2 and M3 with the capacitance C, which is descried in detail [19]. The piecewise linear function (3) can be directly implemented with a current mirror.

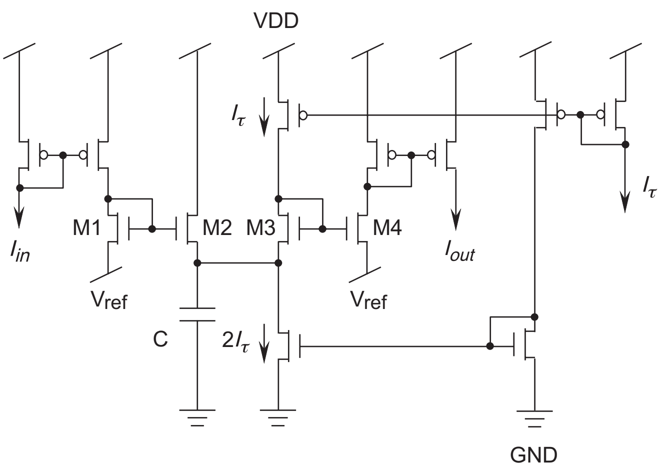

Fig. 4. Schematic of the current-mode low-pass filters.

Fig. 5 is a schematic of a piecewise linear half-center oscillator circuit (hereafter called piecewise linear neuromorphic oscillator) consisting of four current-mode low-pass filters and several current mirrors. The dynamics of the circuit are expressed by the following equations:

$$\tau \frac{\mathrm{d}I_{u_i}}{\mathrm{d}t} = -I_{u_i} + f(I_s - \beta I_{v_i} - wI_{u_j}), \tag{8}$$

$$\tau \frac{\mathrm{d}I_{v_i}}{\mathrm{d}t} = -I_{v_i} + f(I_{u_i}), \tag{9}$$

where I_{u_i} corresponds to the inner state of the ith neuron, I_{v_i} an adaptation variable of the neuron, I_s a tonic input, w_{ij} a synaptic strength between the ith and jth neuron, and β the adaptation effectiveness. The parameters w_{ij} and β are determined by the current transfer ratio of the current mirrors. The time constant τ can be controlled by tuning the bias current I_τ as described in (7). Depending on these circuit parameters, this circuit generates a stable limit-cycle oscillation of the currents I_{u_i} and I_{v_i} corresponding to the state variables u_i and v_i in (4) and (5). Thus, the dynamics of the piecewise linear neuromorphic oscillator are qualitatively the same as that of the piecewise linear half-center oscillator model described by (3)–(5).

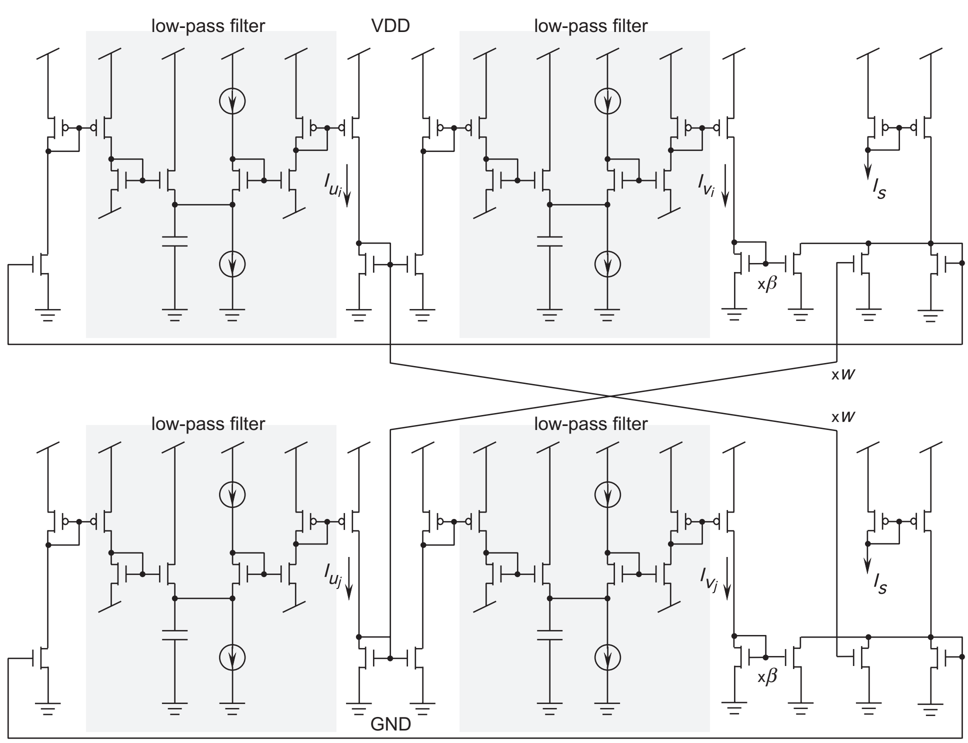

Fig. 5. Schematic of the piecewise linear half-center oscillator circuit.

4. Results

We describe the performance of the piecewise linear neuromorphic oscillator through circuit simulations and experiments on a fabricated chip.

4.1. Simulation results

We simulated the proposed circuit with HSPICE using BSIM 3v3 LEVEL 49 model parameters for AMIS CMOS 1.5-μm process. We set circuit parameters as follows: the capacitance of the current-mode low-pass filters $C = 10\,\text{nF}$, and the power-supply voltages $\text{VDD} = 1.5\,\text{V}$ and $\text{Vref} = 0.35\,\text{V}$. The gate length L of transistors were set at $L = 6.0\,\mu\text{m}$ and the gate width W of the minimum-size transistor was set at $W = 4.5\,\mu\text{m}$

4.1.1. Rhythmic pattern generation

Here, we describe rhythmic pattern generation in the piecewise linear neuromorphic oscillator. Fig. 6A presents the waveforms of the state currents I_{u_i} and I_{v_i}, where the parameters $\beta = 5$ and $w_{ij} = 4$, and the bias currents were set at $I_\tau = 10\,\text{nA}$ and $I_s = 100\,\text{nA}$. The equilibrium currents of the circuit are calculated by solving the following equations:

$$\frac{\mathrm{d}I_{u_i}}{\mathrm{d}t} = \frac{\mathrm{d}I_{v_i}}{\mathrm{d}t} = 0 \quad (i = 1, 2) \tag{10}$$

that yield

$$I_{u_0} = I_s - \beta I_{v_0} - w_{ij} I_{u_0}, \quad I_{v_0} = I_{u_0}, \tag{11}$$

where I_{u_0} and I_{v_0} represent the equilibrium currents. In this simulation, the equilibrium currents were $I_{u_0} = I_{v_0} = I_s/10 = 10\,\text{nA}$. Fig. 6B shows a closed (I_{u_1}, I_{v_1}) phase plane portrait of the circuit. These results confirmed that the circuit generated a stable oscillation.

4.1.2. Frequency and amplitude modulation

The amplitude of the oscillation was proportional to the bias currents I_s as a result of the scaling of the currents I_{u_i} and I_{v_i} due to I_s. We changed the amplitude of the oscillation by tuning I_s from 10 nA at 0 s to 100 nA at 1000 ms as shown in Fig. 6C. We also changed the frequency of the oscillation by tuning the bias current I_τ from 10 nA at 0 s to 50 nA at 1000 ms as shown in Fig. 6D. The controllability of the amplitude and frequency of the oscillation are suitable for a neuromorphic oscillator as a building block for constructing a CPG-based controller.

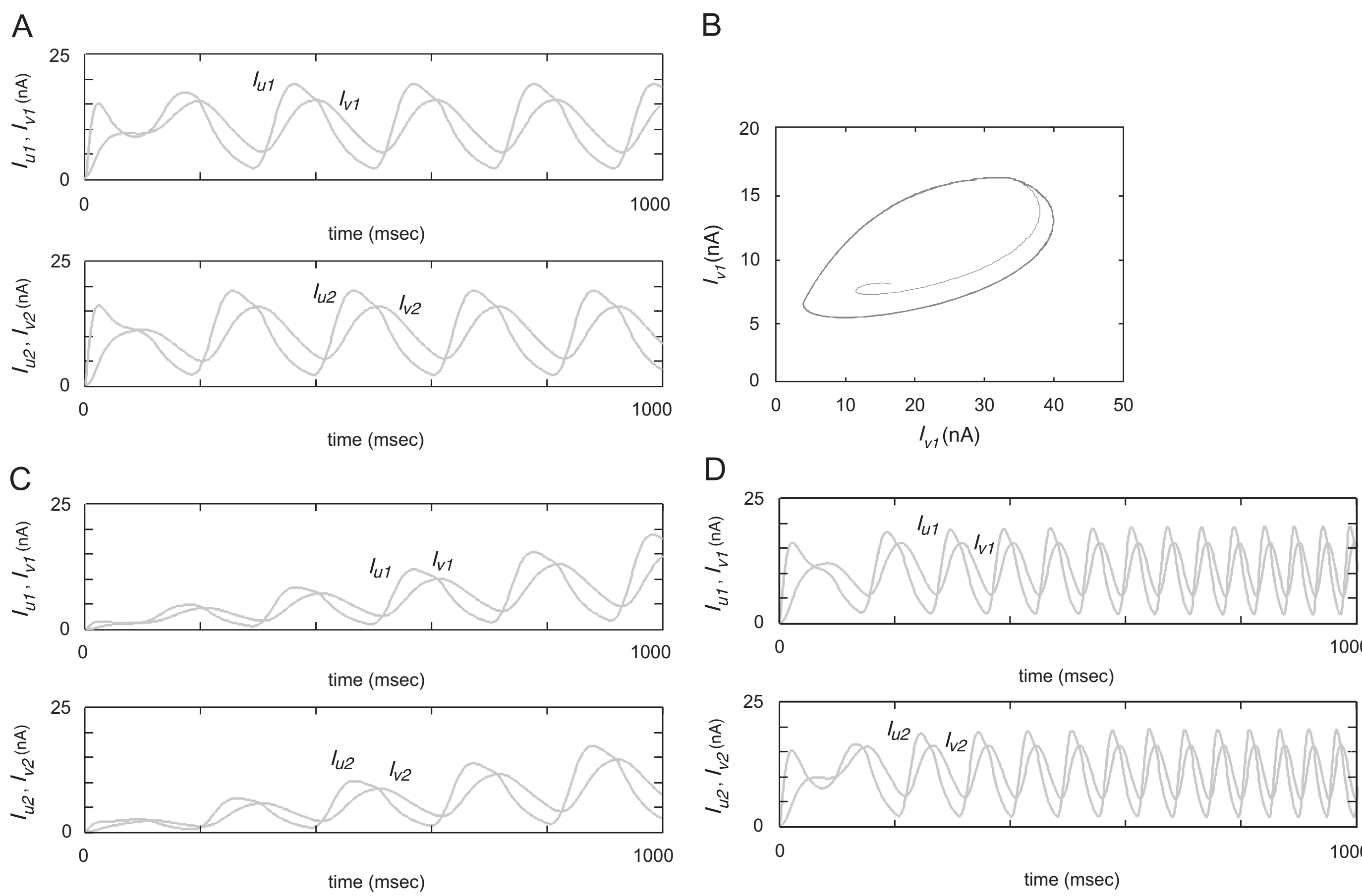

Fig. 6. Simulation results: (A) waveforms of currents and (B) phase plane portrait of the piecewise linear neuromorphic oscillator. (C) Amplitude and (D) frequency modulation by tuning bias currents.

4.2. Experimental results

We designed and fabricated a prototype chip of the proposed circuit with a scalable CMOS rule: MOSIS AMI, n-well double-poly double-metal CMOS process, $\lambda = 0.8\,\mu m$ and feature size: 1.5-μm (Fig. 7). Fig. 8 is a micrograph of the piecewise linear neuromorphic oscillator containing four current-mode low-pass filters and several current-mirrors (chip size: $2.25 \times 2.25\,mm^2$). We set the gate length of the transistors $L = 9.6\,\mu m$. The parameters $\beta = 5$ and $w_{ij} = 4$ were determined by the current transfer ratio of the current mirrors at layout. For measurement, we used the off-chip capacitance $C = 1\,\mu F$ and the supply voltages VDD = 1.5 V and Vrf = 0.35 V.

Fig. 8A presents the waveforms of measured currents I_{u_i} and I_{v_i}, where the bias currents were set at $I_\tau = 100\,nA$ and $I_s = 200\,nA$. Fig. 8B shows a closed (I_{ui}, I_{v_i}) phase plane portrait. These results show that the circuit generates stable oscillation that is qualitatively the same as that of simulation results. However, we found the influence of device mismatch on the oscillation, such as asymmetry in the waveforms of the currents and a distortion in the phase plane portrait.

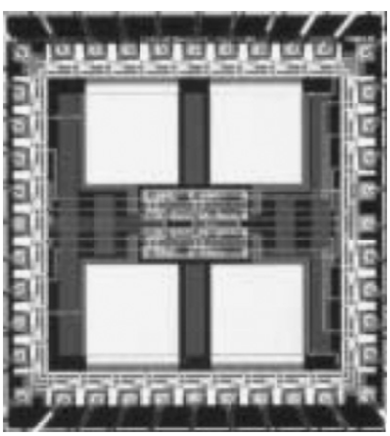

Fig. 7. Micrograph of a fabricated chip.

5. Device mismatch compensation of exploiting physical feedback

Here, we propose a compensation for the influence of the device mismatch of the piecewise linear neuromorphic oscillator exploiting sensory feedback from a coupled physical system.

5.1. Feedback control loop including nonlinear oscillator and physical system

In the following, we consider a feedback control loop including a nonlinear oscillator and a physical system as shown in Fig. 9. Williamson has investigated entrainment properties of such a loop, and applied the entrainment properties for controlling rhythmic arm movements of a humanoid [33]. As a result of the entrainment of the feedback control loop, the amplitude and frequency of oscillation of both the nonlinear oscillator and the physical system are modulated. The necessary condition of the stable oscillation is given by the following equation:

$$|C(s)P(s)| \geqslant 1, \tag{12}$$

where $C(s)$ and $P(s)$ represent transfer functions of the nonlinear oscillator and the physical system, respectively.

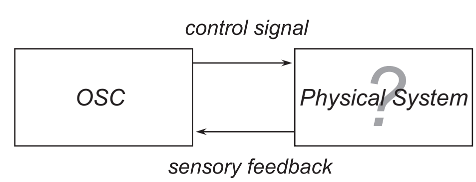

Fig. 9. Block diagram of feedback control loop including nonlinear oscillator (OSC) and physical system.

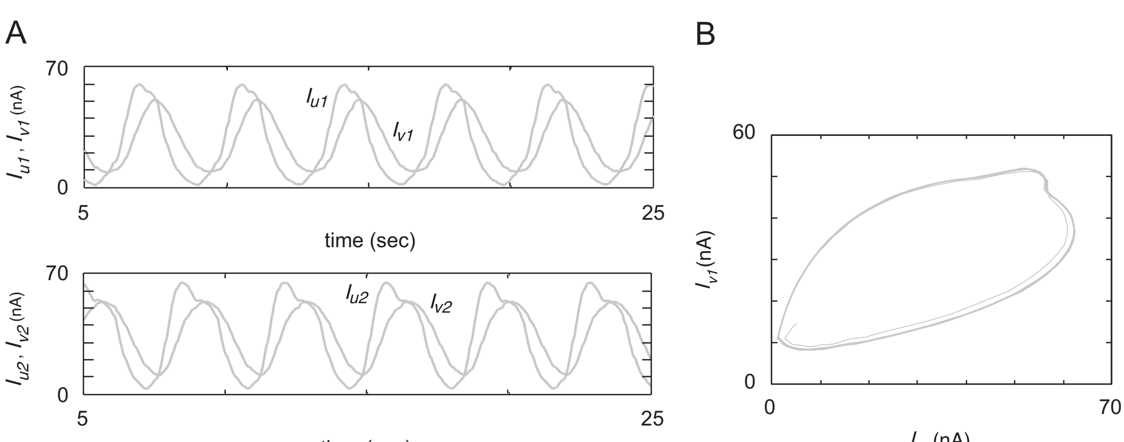

Fig. 8. Experimental results: (A) waveforms of currents and (B) phase plane portrait of the piecewise linear neuromorphic oscillator.

5.2. Reducing influence of device mismatch through physical feedback

We here consider exploiting the transfer characteristics of the feedback control loop to reduce the influence of the device mismatch in the piecewise linear neuromorphic oscillator. The transfer function of the feedback control loop $T(s)$ is described by the following equation:

$$T(s) = \frac{C(s)P(s)}{1 + C(s)P(s)}, \tag{13}$$

where $C(s)P(s)$ is the input loop transfer function. When we regard $C(s)$ as the transfer function of the piecewise linear neuromorphic oscillator, the device deviation of the neuromorphic oscillator can be regarded as the deviation of $C(s)$, namely, $\delta C(s)$. When we differentiate $T(s)$ with respect to s, then we obtain the following equations:

$$\frac{\partial T(s)}{\partial C(s)} = \frac{C(s)}{(1 + C(s)P(s))^2} = \frac{1}{1 + C(s)P(s)} \cdot \frac{T(s)}{C(s)}, \tag{14}$$

that yield

$$\frac{\delta T(s)}{T(s)} = \frac{1}{1 + C(s)P(s)} \cdot \frac{\delta C(s)}{C(s)} = S(s) \cdot \frac{\delta C(s)}{C(s)}, \tag{15}$$

where we assumed that $P(s)$ is invariant. Here, $\delta T(s)$ represents the deviation of $T(s)$, and $S(s)$ the sensitivity function. For reducing the influence of the device deviation of the piecewise linear neuromorphic oscillator $\delta C(s)$ on the transfer characteristics of the entire system, the following condition:

$$|S(s)| = |1 + C(s)P(s)|^{-1} \ll 1 \tag{16}$$

should be satisfied.

5.3. Transfer characteristics of physical system

We here consider a joint actuator with single degree-of-freedom (DOF) as a physical system. The dynamics of the joint actuator is given as follows:

$$M\ddot{\theta} + k\dot{\theta} + c\theta = \tau, \tag{17}$$

where θ is the joint angle, M the moment of inertia of the joint actuator, k the stiffness parameter, and c the damping parameter. We introduce a simple proportional differential (PD) controller generating the driving force τ:

$$\tau = K_P(\hat{\theta} - \theta) - K_D\dot{\theta}, \tag{18}$$

where $\hat{\theta}$ is the equilibrium angle. We assumed that θ and $\dot{\theta}$ can be measured quite accurately. The parameters K_P and K_D represent the proportional and differential parameters, respectively. The physical system including the PD controller (Fig. 10) is regarded as a standard second-order system, then the transfer function of the system $P(s)$ is

Table 1

Parameters	Without feedback	With feedback
ξ	1.0	1.0
ω_n (rad/s)	10	10
G (rad/nA)	0.05	0.02
ζ (nA/rad)	0	0
η (nA s/rad)	500	0

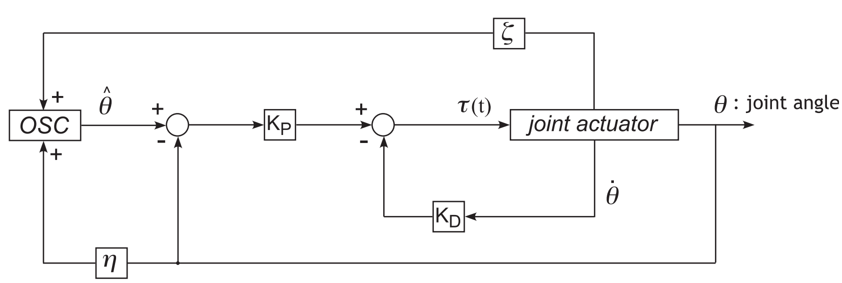

Fig. 10. Configuration of control system including feedback loop D.

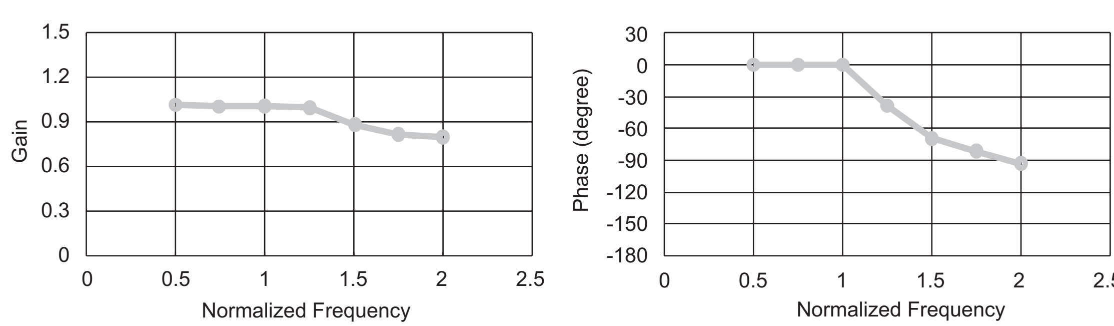

Fig. 11. Transfer characteristics of the piecewise linear neuromorphic oscillator.

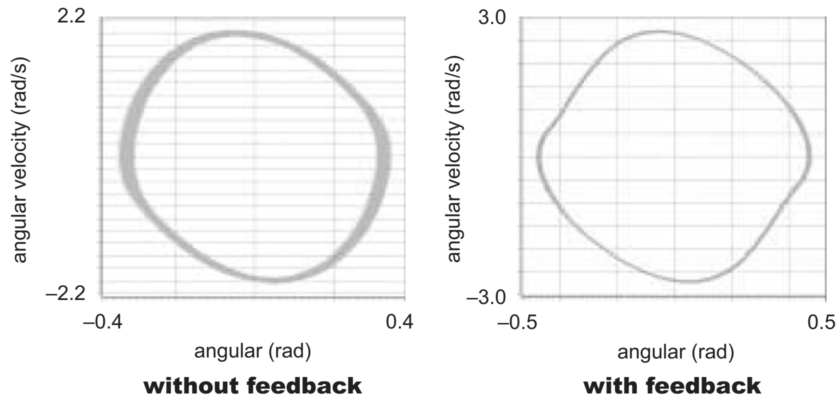

Fig. 12. Physical feedback compensation.

given as follows:

$$P(s) = \frac{\omega_n^2}{s^2 + 2\xi\omega_n s + \omega_n^2}, \quad \xi = \frac{K_D + c}{2\sqrt{M(K_P + k)}},$$
$$\omega_n = \sqrt{\frac{K_P + k}{M}}, \tag{19}$$

where ω_n is the natural angular frequency of the system, and ξ the damping parameter. Thus, $P(s)$ can be regulated by tuning K_P and K_D.

5.4. Transfer characteristics of piecewise linear neuromorphic oscillator

The transfer function of the piecewise linear neuromorphic oscillator $C(s)$ cannot to be derived analytically due to the nonlinearity. Thus, we estimated $C(s)$ from simulation results, such as shown in Fig. 11. The input $I(t)$ was given into the piecewise linear neuromorphic oscillator as follows:

$$\tau \frac{dI_{u_1}}{dt} = -I_{u_1} + f(I_s - \beta I_{v_1} - wI_{u_2} - I(t)), \tag{20}$$

$$\tau \frac{dI_{v_1}}{dt} = -I_{v_1} + f(I_{u_1}), \tag{21}$$

$$\tau \frac{dI_{u_2}}{dt} = -I_{u_2} + f(I_s - \beta I_{v_2} - wI_{u_1} + I(t)), \tag{22}$$

$$\tau \frac{dI_{v_2}}{dt} = -I_{v_2} + f(I_{u_2}) \tag{23}$$

and we defined the output as $I_{out} = I_{u_1} - I_{u_2}$. The transfer function $C(s)$ is determined by the circuit parameters. In particular, the natural frequency is crucial for the entrainment between the neuromorphic oscillator and a physical system.

5.5. Monte-Carlo simulations

We simulated how the physical feedback reduces the influence of the device mismatch on the operation of the feedback control loop through Monte-Carlo simulations using SPICE. We set circuit parameters for the neuromorphic oscillator as follows: $I_\tau = 10\,\text{nA}$, $I_s = 500\,\text{nA}$, $C = 50\,\text{nF}$, $\beta = 5$ and $w = 4$. We tuned the parameters to determine the transfer function of the physical system including the PD controller for satisfying the conditions of (12) and (16), as shown in Table 1. The device deviation of the neuromorphic oscillator was defined as the threshold deviation of transistors: $\sigma(V_{th}) = 0.1\%$.

Fig. 12 shows $(\theta, \dot{\theta})$ phase plane portraits of the joint actuator without and with feedback loop obtained by 100 trials. We here defined the equilibrium angle as $\hat{\theta}_i = G(I_{u_1} - I_{u_2})$, where G is a transformation coefficient, and the physical feedback as $S = \zeta\theta + \eta\dot{\theta}$. These results confirmed that the physical feedback could reduce the influence of the device deviation of the neuromorphic oscillator on the behavior of the joint actuator.

6. Conclusion

We have proposed an analog current-mode subthreshold CMOS circuit for the piecewise linear neuromorphic oscillator model. Our circuit consists of four current-mode low-pass filters and several current mirrors that operate in their subthreshold region under the low-power supply voltages. As a result, low power consumption can be achieved. We have confirmed that the circuit generates stable oscillation and the amplitude and frequency of the oscillation can be controlled by tuning the bias currents. These characteristics of our circuit are suitable as a building block for constructing a CPG-based controller. Furthermore, we have considered how to reduce the influence of the device mismatch on the circuit operation. The compensation method using the physical feedback that we proposed and was confirmed through Monte-Carlo simulations. Further consideration of applying our circuit and compensation method to implement micro robots remains as future work. In particular, low-power consumption of our chip and the physical feedback compensation method are attractive for driving underwater robots that move around unpredictable environments for a long time.

References

[1] A.G. Andreou, K.A. Boahen, P.O. Pouliquen, A. Pavasovic, R.E. Jenkins, K. Strohbehn, Current-mode subthreshold MOS circuits for analog VLSI neural system, IEEE Trans. Neural Network 2 (2) (1991) 205–213.

[2] P. Arena, S. Castorina, L. Fortuna, M. Frasca, M. Ruta, A CNN chip for robot locomotion control, in: Proceedings of the IEEE International Symposium Circuits and Systems, vol. 3, 2003, pp. 510–513.

[3] P. Arena, L. Fortuna, M. Frasca, L. Patane, Sensory feedback in CNN-based central pattern generators, Int. J. Neural Syst. 13 (6) (2003) 469–478.

[4] A.M. Arsenio, On stability and tuning of neural oscillators: application to rhythmic control of a humanoid robot, in: International Joint Conference on Neural Networks, 2004.

[5] M. Branciforte, G. Di Bernardo, F. Doddo, L. Occhipinti, Reaction–diffusion CNN design for a new class of biologically-inspired processors in artificial locomotion applications, in: Seventh International Conference on Microelectronics for Neural, Fuzzy and Bio-Inspired Systems, Granada, Spain, 1999, pp. 69–77.

[6] G. Brown, On the nature of the fundamental activity of the nervous centers: together with an analysis of the conditioning of the rhythmic activity in progression, and a theory of the evolution of function in the nervous system, J. Physiol. 48 (1914) 18–46.

[7] J.J. Collins, S.A. Richmond, Hard-wired central pattern generators for quadrupedal locomotion, Biol. Cybern. 71 (1994) 375–385.

[8] F. Delcomyn, Foundations of Neurobiology, W.H. Freeman, New York, 1997.

[9] M. Golubitsky, I. Stewart, The Symmetry Perspective: From Equilibrium to Chaos in Phase Space and Physical Space, Birkhauser, Basel, 2002.

[10] J. Goncalves, Regions of stability for limit cycles of piecewise linear systems, in: IEEE Conference on Decision and Control, Maui, Hawaii, December 2003.

[11] A.J. Ijspeert, A connectionist central pattern generator for the aquatic and terrestrial gaits of a simulated salamander, Biol. Cybern. 84 (5) (2001) 331–348.

[12] A.J. Ijspeert, Vertebrate locomotion, in: M.A. Arbib (Ed.), The Handbook of Brain Theory and Neural Networks, MIT Press, Cambridge, MA, 2003, pp. 649–654.

[13] H. Kimura, Y. Fukuoka, K. Konaga, Adaptive dynamic walking of a quadruped robot by using neural system model, Adv. Robot. 15 (8) (2001) 859–876.

[14] S. Kotosaka, S. Schaal, Synchronized robot drumming by neural oscillator, J. Robot. Soc. Japan 1 (2001) 116–123.

[15] M.A. Lewis, M.J. Harttmann, R. Etienne-Cummings, A.H. Cohen, Control of a robot leg with an adaptive a VLSI CPG chip, Neurocomputing 38–40 (2001) 1409–1421.

[16] M. Lungarella, L. Berthouze, Robot bouncing: on the interaction between neural and body-environment dynamics, in: F. Iida, R. Pfeifer, L. Steels, Y. Kuniyoshi (Eds.), Embodied Artificial Intelligence, Springer, Berlin, 2004.

[17] K. Matsuoka, Sustained oscillations generated by mutually inhibiting neurons with adaptation, Biol. Cybern. 52 (1983) 367–376.

[18] K. Matsuoka, Mechanism of frequency and pattern control in the neural rhythm generators, Biol. Cybern. 56 (1987) 345–353.

[19] A. McEwan, A. van Schaik, An analogue VLSI implementation of the Meddis inner hair cell model, EURASIP J. Appl. Signal Process. 7 (2003) 639–648.

[20] T. Mori, Y. Nakamura, M. Sato, S. Ishii, Reinforcement learning for CPG-driven biped robot, in: Proceedings of the Nineteenth National Conference on Artificial Intelligence, 2004, pp. 623–630.

[21] J. Mulder, A.C. van der Woerd, W.A. Serdijn, H.M. van Roermund, General current-mode analysis method for translinear filters, IEEE Trans. Circuits Syst. I 44 (1997) 193–197.

[22] K. Nakada, T. Asai, Y. Amemiya, An analog CMOS central pattern generator for interlimb coordination in quadruped locomotion, IEEE Trans. Neural Networks 14 (5) (2003) 1356–1365.

[23] K. Nakada, T. Asai, Y. Amemiya, Analog CMOS implementation of a CNN-based locomotion controller with floating-gate devices, IEEE Trans. Circuits Syst. I 52 (6) (2005) 1095–1103.

[24] J. Nakanishi, J. Morimoto, G. Endo, G. Cheng, S. Schaal, M. Kawato, An empirical exploration of phase resetting for robust biped locomotion with dynamical movement primitives, in: Proceedings of the IEEE/RSJ International Conference on Intelligent Robots and Systems, 2004, pp. 919–924.

[25] K. Ohgane, S. Ei, K. Kazutoshi, T. Ohtsuki, Emergence of adaptability to time delay in bipedal locomotion, Biol. Cybern. 90 (2) (2004) 125–132.

[26] G. Patel, J. Holleman, S. DeWeerth, Analog VLSI model of intersegmental coordination with nearest-neighbor coupling, Adv. Neural Inf. Process. Syst. 10 (1998) 710–725.

[27] S. Ryckebusch, J.M. Bower, C.A. Mead, Modeling small oscillating biological networks in analog VLSI, Adv. Neural Inf. Process. Syst. 1 (1989) 384–393.

[28] S. Still, K. Hepp, R.J. Douglas, Neuromorphic walking gait control, IEEE Trans. Neural Networks 17 (2) (2006) 496–508.

[29] S. Still, M.W. Tilden, Controller for a four legged walking machine, in: L.S. Smith, A. Hamilton (Eds.), Neuromorphic Systems Engineering Silicon from Neurobiology, World Scientific, Singapore, 1998, pp. 138–148.

[30] G. Taga, A model of the neuro-musculo-skeletal system for anticipatory adjustment of human locomotion during obstacle avoidance, Biol. Cybern. 78 (1) (1998) 9–17.

[31] G. Taga, Y. Yamaguchi, H. Shimizu, Self-organized control of bipedal locomotion by neural oscillators in unpredictable environment, Biol. Cybern. 65 (1991) 147–159.

[32] F. Tenore, R. Etienne-Cummings, M.A. Lewis, A programmable array of silicon neurons for the control of legged locomotion, Presented at IEEE International Symposium Circuits and Systems, Vancouver, 2004.

[33] M. Wiliamson, Neural control of rhythmic arm movements, Neural Networks 11 (7–8) (1998) 1379–1394.

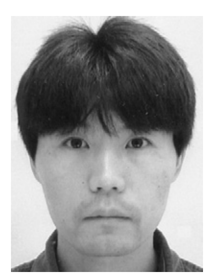

Kazuki Nakada received his B.S., M.S., and Ph.D. degrees from Hokkaido University, Sapporo, Japan, in 1999, 2002, and 2005, respectively. Currently, he is a Research Associate in Kyushu Institute of Technology, Kitakyushu, Japan. His research interests are in the field of neuromorphic VLSI systems as well as biologically inspired robotics and concentrate on development of noise robust VLSI systems exploiting neurodynamics.

Tetsuya Asai received his B.E. and M.E. degrees in electrical engineering from Tokai University, Kanagawa, Japan, in 1993 and 1996, respectively, and the Dr. Eng. degree in electrical and electronic engineering from Toyohashi University of Technology, Aichi, Japan, in 1999. He is an Associate Professor in the Graduate School of Information Science and Technology, Hokkaido University, Sapporo, Japan. His research interests concentrate on developing nature-inspired integrated circuits and their computational applications. Current topics that he is involved with include intelligent image sensors that incorporate biological visual systems or cellular automata in the chip, neuro chips that implement neural elements (neurons, synapses, etc.) and neuromorphic networks, and reaction–diffusion chips that imitate vital chemical systems.

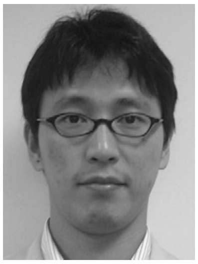

Tetsuya Hirose received his B.S., M.S., and Ph.D. degrees from Osaka University, Osaka, Japan, in 2000, 2002, and 2005, respectively. Currently, he is a Research Associate in the Department of Electrical Engineering, Hokkaido University, Sapporo, Japan. His current research interests are in low-power analog/digital CMOS circuits and subthreshold MOSFET functional circuits for intelligent sensors. Dr. Hirose is a member of the Institute of Electronics, Information and Communication Engineers of Japan, and the IEEE.

Hatsuo Hayashi received his B.E., M.E., and Ph.D. degrees from Kyushu University, Fukuoka, Japan, in 1971, 1973, and 1983, respectively. He was an assistant professor of the Department of Electronics, Kyushu University, Fukuoka, from 1976 to 1986, where he worked on chaotic nature of single molluscan neurons, and was an associate professor of the Department of Computer Science and Electronics, Kyushu Institute of Technology, Iizuka, Japan, from 1987 to 1999, where he worked on chaotic responses of the mammalian brain (hippocampus and sensory cortex) and dynamical features of models of the molluscan neuron and the hippocampal network. He was a professor of the Department of Computer Science and Electronics, Kyushu Institute of Technology, in 2000. Since 2001, he has been a professor of the Department of Brain Science and Engineering, Kyushu Institute of Technology, Kitakyushu, Japan. He is recently taking a great interest in memory and learning functions of the hippocampus and the entorhinal cortex, besides their neurodynamics. He was also a research associate of the Department of Physiology and Biophysics, University of Texas, Galveston, from 1984 to 1985, and the Department of Molecular and Cell Biology, University of California, Berkeley, in 1991.

Yoshihito Amemiya received B.E., M.E., and Dr. Eng. degrees from the Tokyo Institute of Technology, Tokyo, Japan, in 1970, 1972, and 1975, respectively. He joined NTT Musashino Laboratories in 1975, where he worked on the development of silicon process technologies for high-speed logic LSIs. From 1983 to 1993, he was with NTT Atsugi Laboratories and developed bipolar and CMOS circuits for Boolean and non-Boolean logic LSIs. Since 1993, he has been a Professor with the Department of Electrical Engineering, Hokkaido University, Sapporo. His research interests are in the fields of silicon LSI circuits, signal processing devices based on nonlinear analog computation, logic systems consisting of single-electron circuits, and information-processing devices making use of quantum nanostructures.